ANALYSIS OF VELOCITY AND TEMPERATURE FIELDS OF MOLTEN METAL IN DC ELECTRIC ARC FURNACE

HIDEKAZU KURIMOTO*
Department of Natural Science Informatics, Nagoya University, Furo-cho, Chikusa-ku, Nagoya 464-01, Japan
HARENDRA NATH MONDAL, TOSHIYA MORISUE
Department of Chemical Engineering, Nagoya University, Furo-cho, Chikusa-ku, Nagoya 464-01 Japan

Key Words: DC Arc Furnace, Numerical Simulation, Process Modelling Navier-Stokes Equations, Magnetohydrodynamics

Recently some small scale industries have started using DC electric arc furnace to recycle scrap materials, however modelling and simulation data are very limited in the literature. Therefore, it appears that a numerical simulation could provide many important components for predicting suitable operating conditions, better design and efficient control of the process. With this objective, a numerical simulation model is developed under certain simplifying assumptions. A SIMPLER algorithm is used to solve the model equations.

Computed results show that the circulating patterns and the patterns of increasing the temperature of the melt are significantly affected by the change in bottom electrode diameter and these calculated results present very important information. For example, a furnace can be designed in such a way that the melt temperature can be increased uniformly throughout the bath which is very important for making homogeneous alloys. It is also found that the effect of natural convection on melt circulation is negligible, that is, circulation is totally controlled by the electromagnetic force field. In addition to the flow field data, data obtained from the electromagnetic field computations are also presented.

Introduction

In developed countries, automobile and metallurgical equipment manufacturing industries are under pressure to recycle used vehicles and equipment, primarily because of shortages of energy and resources and pollution of the environment. Some small scale industries have begun using the DC electric arc furnace to recycle scrap materials. DC arc furnaces are usually characterized by a centrally positioned graphite electrode which acts as the cathode. It has several advantages over AC arc furnaces. For example, an AC arc burns at an angle and is forced by the electromagnetic field towards the furnace wall, causing undesirable hot spots. In contrast, DC arc burns vertically and as a result, a high portion of the DC arc heat is delivered directly to the melt. Another important advantage is the reduction of the electrode-tip erosion rate (almost 40% tip-erosion rate is reduced for a DC arc furnace).

In a DC arc furnace, electrically induced flow (EIF) plays a very important role, and it is essential to analyze the flow phenomena to completely understand the process. The major stumbling block to our understanding of kinetics, particularly in the molten state, has been the insufficiency of information about the flow phenomena in these types of systems. When the flow field is not known, the convective heat and mass transfer processes that take place within the system have to be represented in terms of empirical transport coefficients, which rather than being general are necessarily specific to given situations. This in turn may hamper the fundamental understanding of the problems involved. Therefore, it appears that a better understanding of fluid flow and heat transfer phenomena in DC electric arc furnaces could provide an important component for better design and efficient control of the process.

EIF differs from ordinary hydrodynamic flow, because EIF is driven by rotational body forces instead of being a result of imposed inhomogeneous boundary conditions of velocity and pressure. The hydrodynamic effects are due to the interaction of an electric current passing through the fluid with its own magnetic field. The actual flow within the molten metal is caused by a number of driving forces, which include the electromagnetic force field generated by the arc, natural convection due to temperature gradients in the melt, and the interaction between the arc jet (plasma) and the bath. All of these phenomena exist in a DC arc furnace.

Ushiro *et al.* (1981) developed a mathematical formulation to represent the electromagnetic force field, the velocity field and the temperature field in high-current DC arcs. However, they didn't consider the molten metal domains. Szekely *et al.* (1983) were the first to develop a mathematical model to represent heat and fluid-flow phenomena in electric arc furnaces and DC plasma furnaces. But they neglected the effect of the electromag-

* Received on June 30, 1995. Correspondence concerning this article should be addressed to H. Kurimoto.
Autumn meeting of the society of chemical engineers, Japan, September, 1994.

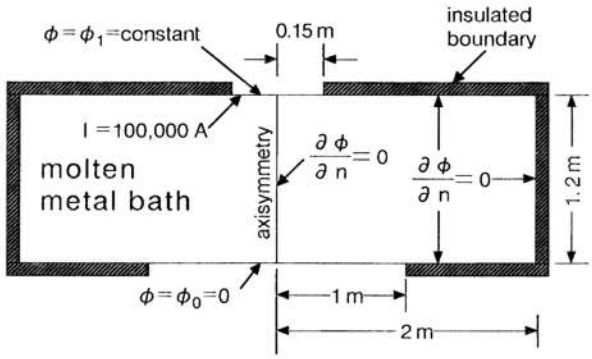

Fig.1 Model of cylindrical DC electric arc furnace

netic force to analyze the temperature field in the molten metal domains. From an industrial standpoint, Yamada *et al.* (1991) developed a model of the IHI-ABB type of furnace. But they didn't include the temperature field in their formulation. Hidaka *et al.* (1991), in a technical report, considered the effect of bottom blown gas, thermal convection, and the effect of the arc jet. However, they analyzed each mathematical model independently, and like Szekely *et al.* (1983) they neglected the effect of electromagnetic force to analyze thermal convection in the molten metal domains.

In this paper, an attempt has been made to develop a numerical simulation model considering simultaneously the magnetohydrodynamic and thermodynamic effects to explain the flow field and the temperature field of a DC arc furnace. Effects of different values of parameters are also investigated.

1. DC arc furnace model

The geometry of the simplified model, and the dimensions as well as boundary conditions regarding ϕ are shown in **Fig. 1**. A DC arc furnace, as shown in Fig. 1, consists of a cylindrical metal bath and its container, a power source, and top and bottom electrodes which are not shown in the figure. An arc is generated at the top electrode and impinges on the bath surface. ϕ_1 represents the potential on the bath surface, not the potential applied at the top electrode. The potential at the bottom electrode and at the bottom surface of the bath ϕ_0 is taken as zero. Symbol $\boldsymbol{I}$ represents the total current entering into the bath. The value of $\boldsymbol{I}$ and all physical dimensions are assumed as trial values.

The following assumptions are made for the numerical simulation:

(a) In this model the fluid is considered as Boussinesq-incompressible (Bejan, 1984), in other words, ρ is constant everywhere except in the body force term of the z-momentum equation where it is replaced by $\rho[1-\beta(T-T_0)]$ and only by this term the temperature field and the flow field are coupled.

(b) It is assumed that arc jet momentum transfer is negligible, that is, the hydrodynamic field within the melt and the shape of the free surface is not disturbed by the arc jet.

(c) Electric current induced due to convective motion of the melt is neglected. Then, the electromagnetic force field and flow field can be calculated separately.

(d) Free surface is assumed as steady and flat.

(e) No physical property variations with temperature except density.

(f) Axisymmetry

At this stage it may be worthwhile to comment on the appropriateness of assumptions (b), (c) and (d).

(b) Consideration of jet momentum can produce a maximum (upward) point velocity which is less than 0.2 meter per second (Szekely *et al.*, 1983). In our case, electromagnetic force produces a maximum (downward) point velocity which is greater than 2.2 meters per second. Hence, compared to the effect of the electromagnetic force, the effect of the jet momentum can be neglected.

(c) Our numerical results show that the magnetic Reynolds number ($Re_m=U_0L_0\sigma\mu_0$), which is a measure of the ratio magnetic convection/magnetic diffusion is approximately equal to 0.017, which is much smaller than unity. Hence assumption (c) also appears to be justified.

(d) Prior to this work, the dynamics of the free surface ware investigated, and it was found that distortion of the free surface was insignificant (Morisue *et al.*, 1994).

The evaluation of the electromagnetic body force, $\boldsymbol{f}_e$, involves two steps. The first step is a solution of current density $\boldsymbol{j}$ in the fluid volume. In general, a boundary value problem for the potential ϕ of the electric field should be solved to find the distribution of $\boldsymbol{j}$. Since current induced by the convective motion of the melt is neglected, the steady current field determination, as shown later, is reduced to the solution of Laplace's equation with appropriate boundary conditions. The next step is the evaluation of the magnetic field induction by the known current density distribution. Usually the magnetic field is evaluated either by using the Biot-Savart law or by Maxwell's curl equation. But for an axisymmetric problem, it is convenient to use Ampere's law.

After field $\boldsymbol{B}$ is found, the electromagnetic force can be evaluated at any point at which the current density $\boldsymbol{j}$ is specified.

In this study, when Ampere's law is applied to calculate the magnetic field induction, the integral regions are taken as full cylinders, whereas differential regions are taken as half cylinders.

The governing equations can be written as follows:

$$\mathrm{curl}\,\boldsymbol{E}=\boldsymbol{0} \tag{1}$$

$$\mathrm{curl}\,\boldsymbol{H}=\boldsymbol{j} \tag{2}$$

$$\mathrm{div}\,\boldsymbol{E}=0 \tag{3}$$

$$\mathrm{div}\,\boldsymbol{B}=0 \tag{4}$$

The above four equations are known as Maxwell's equations. The relation between $\boldsymbol{B}$ and $\boldsymbol{H}$ is given by

$$\boldsymbol{B}=\mu_0\boldsymbol{H} \tag{5}$$

where μ_0 is the permeability of the medium.

Ohm's law

$$\boldsymbol{j} = \sigma \boldsymbol{E} \tag{6}$$

The electromagnetic force is given by

$$\boldsymbol{f}_e = \boldsymbol{j} \times \boldsymbol{B} \tag{7}$$

Since the curl of a gradient is always zero, from Eq. (1), $\boldsymbol{E}$ can be written as

$$\boldsymbol{E} = -\operatorname{grad} \phi \tag{8}$$

where ϕ is called the scalar electric potential. The negative sign implies that the direction of the electric field $\boldsymbol{E}$ is in the direction of decreasing potential. From Eqs. (8) and (3) we get the Laplace's equation, which in cylindrical coordinates is given by

$$\nabla^2 \phi = \frac{\partial^2 \phi}{\partial r^2} + \frac{\partial^2 \phi}{\partial z^2} + \frac{1}{r}\frac{\partial \phi}{\partial r} = 0 \tag{9}$$

Ampere's law

$$\oint \boldsymbol{H} \cdot \boldsymbol{dl} = \int_s \boldsymbol{j} \cdot \boldsymbol{n}\, dS \tag{10}$$

This equation is the integral form of Eq. (2). In this study, the integral form is used. Equation (2) is written for completeness of Maxwell's equations.

The fluid equations to be solved are the Navier-Stokes equations, which in cylindrical coordinates become (in the divergence form):

r-component

$$\rho\left[\frac{\partial u}{\partial t} + \frac{1}{r}\frac{\partial}{\partial r}(ruu) + \frac{\partial}{\partial z}(wu)\right] = -\frac{\partial p}{\partial r} + \mu\left[\frac{\partial}{\partial r}\left(\frac{1}{r}\frac{\partial}{\partial r}(ru)\right) + \frac{\partial^2 u}{\partial z^2}\right] + \rho g_r + [f_e]_r \tag{11}$$

z-component

$$\rho\left[\frac{\partial w}{\partial t} + \frac{1}{r}\frac{\partial}{\partial r}(ruw) + \frac{\partial}{\partial z}(ww)\right] = -\frac{\partial p}{\partial z} + \mu\left[\frac{1}{r}\frac{\partial}{\partial r}\left(r\frac{\partial w}{\partial r}\right) + \frac{\partial^2 w}{\partial z^2}\right] + \rho g_z + [f_e]_z \tag{12}$$

equation of energy

$$\rho c_p\left[\frac{\partial T}{\partial t} + \frac{1}{r}\frac{\partial}{\partial r}(ruT) + \frac{\partial}{\partial z}(wT)\right] = k\left[\frac{1}{r}\frac{\partial}{\partial r}\left(r\frac{\partial T}{\partial r} + \frac{\partial^2 T}{\partial z^2}\right)\right] + \frac{j^2}{\sigma} \tag{13}$$

and the continuity relation is

$$\frac{1}{r}\frac{\partial}{\partial r}(ru) + \frac{\partial w}{\partial z} = 0 \tag{14}$$

Boundary conditions:

At the top surface,

$$\frac{\partial u}{\partial z} = w = 0, \quad \frac{\partial \phi}{\partial z} = 0, \quad \text{and} \quad \frac{\partial T}{\partial z} = 0 \tag{15}$$

Near the top electrode (within the arc spot radius),

$$\frac{\partial u}{\partial z} = w = 0, \quad -k\frac{\partial T}{\partial z} = q \quad \text{and} \quad \phi = \text{constant} \tag{16}$$

At the bottom surface,

$$u = 0, \quad w = 0, \quad \frac{\partial \phi}{\partial z} = 0 \quad \text{and} \quad \frac{\partial T}{\partial z} = 0 \tag{17}$$

Within the bottom electrode diameter,

$$u = w = 0, \quad k\frac{\partial T}{\partial z} = 0, \quad \text{and} \quad \phi = 0 \tag{18}$$

At the right wall and also at the symmetric axis,

$$\frac{\partial \phi}{\partial r} = 0 \quad \text{and} \quad \frac{\partial T}{\partial r} = 0,$$
$$u = w = 0 \quad \text{right wall}, \quad u = \frac{\partial w}{\partial r} = 0 \quad \text{symmetric axis} \tag{19}$$

Numerical simulation involves the following steps in order:

Step 1:Equation (9) is solved to get the scalar potential distribution.

Step 2:Using Eq. (8), electric field $\boldsymbol{E}$ is calculated.

Step 3:Using Eq. (6), current density $\boldsymbol{j}$ is calculated.

Step 4:Using Eq. (10), magnetic field $\boldsymbol{H}$ is evaluated. Here it should be noted that when Eq. (10) is used, the integral regions are taken as full cylinders. In this axisymmetric problem, the magnetic field has only one component, i.e., the θ component. Therefore, Eq. (10) takes the following form:

$$2\pi L H_\theta(z, L) = \int_0^L j_z(z, \acute{r})\, 2\pi \acute{r}\, d\acute{r} \tag{20}$$

Here L represents the radial distance where $\boldsymbol{H}$ is sought.

Step 5:Using Eqs. (5) and (7), the electromagnetic force is computed. Then, using these electromagnetic body forces, Eqs. (11), (12), (13) and (14) are solved simultaneously.

All computations are performed for molten steel. The initial temperature of the melt is assumed close to the melting temperature (1873K). The values of parameters used in this study are taken from previous theoretical and experimental works (Yamada *et al.*, 1991; Nakamura *et al.*, 1991). Electrical permeability and conductivity are taken as $4\pi \times 10^{-7}$ H/m and 1.4×10^6 ℧/m respectively. Density and viscosity are taken as 7010 kg/m^3 and 10 mPas respectively. Coefficient of thermal expansion β [K^{-1}], thermal conductivity k [W/m K] and specific heat at constant pressure c_p [J/Kg K] are taken as 0.001, 100 and 710, respectively. Different values of heat flux at the surface (below the top electrode) q [W/m^2] are considered (2×10^4, 4×10^4 and 6×10^4). Different values of total current $\boldsymbol{I}$ (40,000 amperes, 50,000 amperes, and 100,000 amperes), as well as several values of bottom electrode diameters (0.30m, 1.0m and 2.0m) are also considered.

2. Solution Technique

A control volume based finite difference technique was used to solve the model equations with appropriate boundary conditions. The governing partial differential

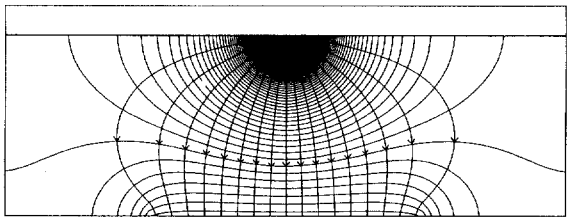

(a) Top electrode diameter is 0.30m and bottom electrode diameter is 2m. Potential at the top surface (ϕ_1 in Fig. 1) is 130 mvolts.

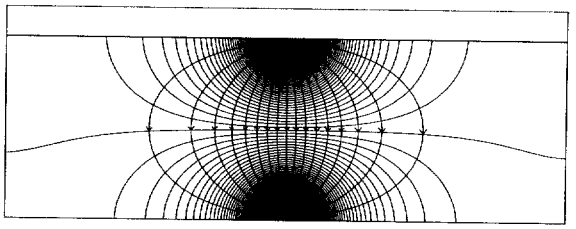

(b) Both the top and bottom electrode diameters are 0.30m. Potential at the top surface (ϕ_1 in Fig. 1) is 240 mvolts.

Fig. 2 Calculated equi-potential lines and current flow lines

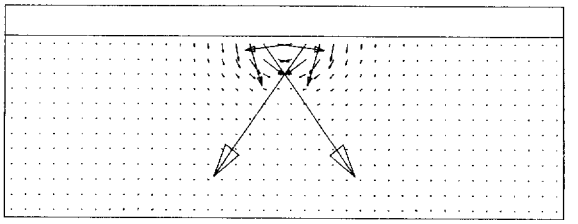

(a) Top electrode diameter is 0.30m and bottom electrode diameter is 2m. Maximum value of force becomes 62,285 N/m^3.

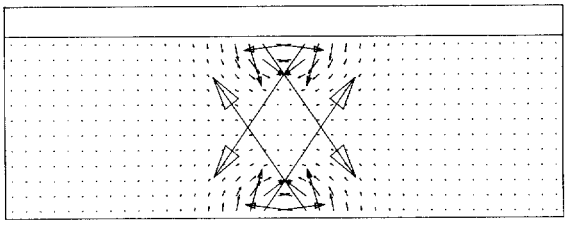

(b) Both the top and bottom electrode diameters are 0.30m. Maximum value of force becomes 62,431 N/m^3.

Fig. 3 Calculated electromagnetic force field

equations are converted to systems of algebraic equations through an appropriate integration over each control volume of the domain and finite difference approximation of partial derivatives. The SIMPLER algorithm was used to solve the equations in primitive variables (Patankar, 1980).

The number of grids used for calculation of the flow field is 40×24, and that for the force field is 80×48. For accuracy, these mesh sizes were chosen small enough to resolve the expected spatial variations in all dependent variables. As fluid can not move through more than one cell in one time step because the difference equations assume fluxes only between adjacent cells, the choice of a mesh size controls the time-step necessary for stability (Courant condition). In most cases, the Courant limitation is the determining factor, and it is only in the case of very low velocity that the time step sizes associated with the viscous terms and the thermal conduction terms may become limiting factors. In this case the Courant condition becomes

$$\Delta t < \Delta t_{Cou} \approx \left[\left(\frac{\Delta x_i}{u_i}\right)_{\min}, \left(\frac{\Delta z_i}{w_i}\right)_{\min}\right]_{\min} \tag{21}$$

As a result, calculation of the flow field requires a long computational time because the large magnitude of electromagnetic force requires a small time-step to obtain a stable solution. In this work, the value of the time step used was 0.001 second, and one time step calculation needed approximately 4 seconds on a HP work station (17.9 Mflops).

3. Computed Results

The value of the electric potential ϕ_1 at the top surface (in Fig. 1) is estimated by trial and error such that total current flowing through the arc furnace becomes approximately equal to some prespecified value. The calculated value of ϕ_1 becomes less than 1 volt, that is, more than 99% of the applied potential drops within the arc.

Figure 2 shows the equi-potential lines and current flow lines for both small and large bottom electrode diameters. These two figures show that equi-potential lines and current flow lines are very concentrated near the top in the case of a large bottom electrode, and near the top and bottom electrodes in the case of a small bottom electrode. Therefore, as shown in **Fig. 3**, the electromagnetic forces become large in these areas. Electromagnetic forces are much greater in magnitude near the small electrodes compared to other areas.

True steady state does not exist in a DC arc furnace because the temperature continues to increase with time, however, almost pseudo-steady state with respect to velocity is attained approximately in 15 seconds for a small bottom electrode and in 22 seconds for a large bottom electrode when total current flowing through the bath is 100,000 amperes.

As buoyant force, generated by the density difference, is very small in comparison to the electromagnetic force, the flow pattern is governed by the electromagnetic force. In Fig. 3(a), forces of large magnitude are concentrated near the top electrode. Because of this, most of the melt rotates in the same direction as shown in **Fig. 4**. In Fig. 3(b),

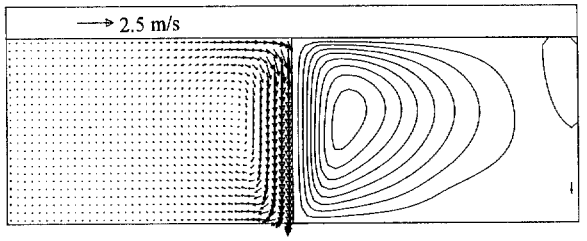

(a) After 2 seconds

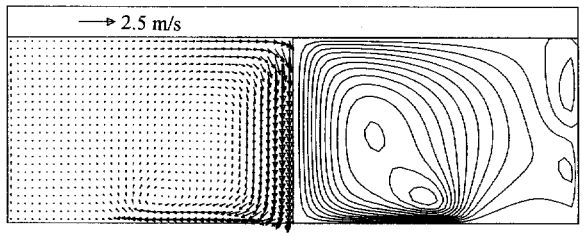

(b) After 5 seconds

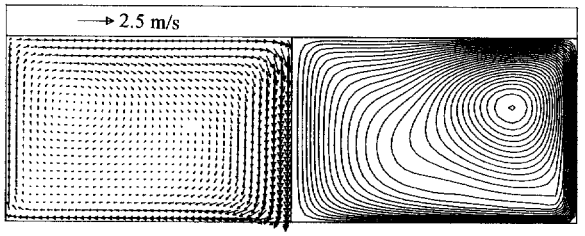

(c) After 22 seconds

Fig. 4 Calculated velocity distributions and stream functions as a function of time. Top electrode diameter is 0.30m and bottom electrode diameter is 2m. Time step used for calcilation is 0.001 sec

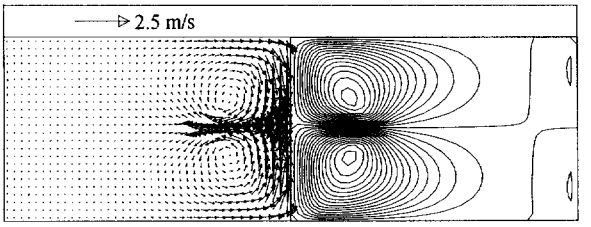

(a) After 2 seconds

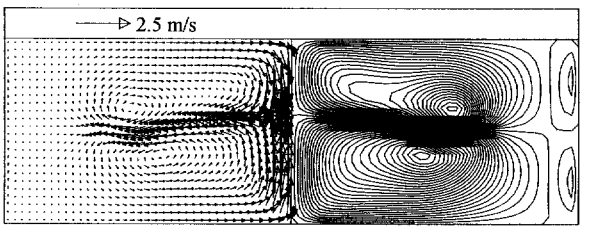

(b) After 5 seconds

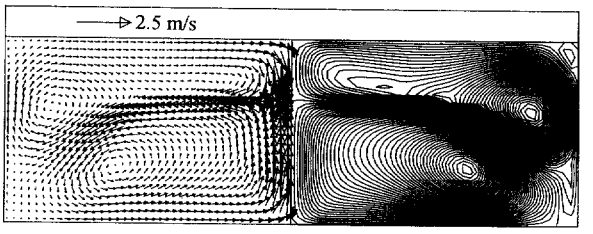

(c) After 15 seconds

Fig. 5 Calculated velocity distributions and stream functions as a function of time. Both top and bottom electrode diameters are 0.30m. Time step used for calculation is 0.001 sec

forces of large magnitude are concentrated near the top and bottom electrodes, and these forces are equal in magnitude but opposite in direction. Then, two main vortical regions are generated with opposite rotation as shown in **Fig. 5**.

Figures 6 and **7** show how the isotherms are developing with time. Comparing the isotherms of Figs. 6 and 7 with stream functions of Figs. 4 and 5, it is found that the isotherms are parallel to the stream functions. This is because the heat supplied to the bath surface is convected into the melt by the fluid and the role of conduction in insignificant. If the heat is supplied to the top surface without the presence of the electromagnetic force, fluid should move from the symmetric axis towards the walls along the top surface, i.e., a clockwise circulation should appear because low density fluid appears near the top surface. However, in the DC arc furnace, electromagnetic force totally suppresses the natural convection and helps to increase the temperature uniformly by forced convection within a vortical region of the melt.

Figure 7 shows that the isotherms are not reaching the bottom region when the bottom electrode diameter is small but Fig. 6 shows that the isotherms are reaching the bottom region when the bottom electrode diameter is large. On the other hard, Fig. 2 shows the current density in the bottom region is much greater for small bottom electrode in comparison to large bottom electrode. This explains two facts. One is that the electrical heat generation within the melt (j^2/σ) is not significant, that is, the source of the isotherms is the heat supplied at the bath surface. Another one is that it is not possible to increase the temperature in the bottom part of the melt when the bottom electrode diameter is small because two separating layers of opposite rotation prevent the convection from the upper part to the lower part.

Simulation is also performed for different values of total current I and surface heat flux q. When total current I is reduced, only the magnitude of electromagnetic forces decreases, and vice versa. As a result, the velocity field and the temperature fields develop slowly without affecting the pseudo-steady state flow configuration. On the other hand, changing the value of q only results in a relative increase or decrease in temperature in the molten metal bath. Its influence on the flow fields and on the convective heat transfer patterns (pattern of isotherms) are insignificant.

Numerical calculation is also performed for different bottom electrode diameters (0.30 m, 1.0 m and 2.0 m). But ultimately, in the pseudo-steady state condition either two main vortical regions (for 0.30 m) or a single vortical region (for 1.0 m and 2.0 m) is generated. It is also found that a single clockwise circulating pattern is generated when the bottom electrode diameter is chosen much smaller than

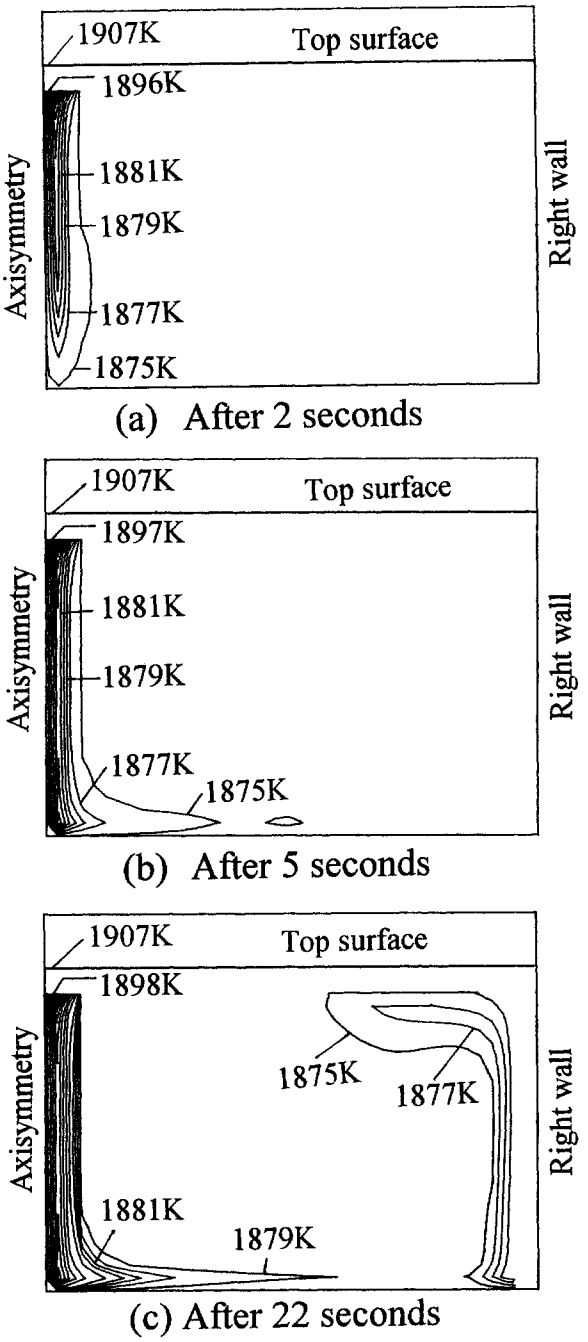

Fig. 6 Change in isotherms at different times for large bottom electrode diameter (2m). Surface heat flux q is taken as 2×10^4 W/m^2

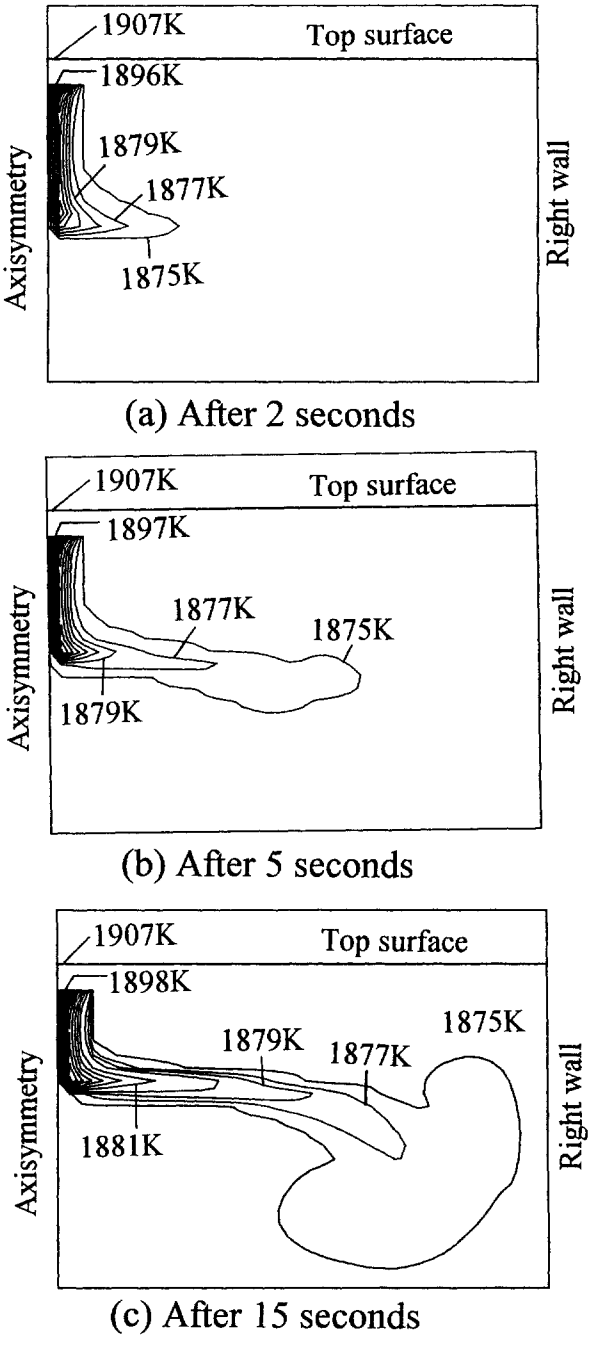

Fig. 7 Change in isotherms at different times for small bottom electrode diameter (0.30m). Surface heat flux q is taken as 2×10^4 W/m^2

the top electrode diameter (result is not shown due to space limitation).

Since we do not have real process data, we can not compare our results with practical ones. It would be necessary to verify the results for further research. Although it is obvious that the shape of the electrode (arc), radius or dimension of the arcspot and changing position of the arc with respect to time would significantly affect the velocity and temperature fields, we will consider the three dimensional nature of the problem in the next step of our research.

Conclusion

A numerical simulation model is developed considering the thermo- and magnetohydrodynamic effects to explain the flow and the temperature field of a DC arc furnace. A SIMPLER algorithm is used to solve the model equations. Calculated results show that the melt circulating patterns vary significantly as the bottom electrode diameter is changed. Since the heat supplied at the surface by the arc penetrates into the melt along the stream lines, i.e., supplied heat is carried inside the melt by the fluid

motion, the temperature distribution within the melt can be predicted or controlled by suitable design of the electrodes. The effects of different values of surface heat flux, total current and bottom electrode diameters are investigated, and it was found that the influences of total current and bottom electrode diameter on the flow field are more significant compared with the value of surface heat flux.

Nomenclature

$\boldsymbol{B}$	=	magnetic flux density	[Wb.m^{-2}]
c_p	=	specific heat at constant pressure	[J.kg^{-1}.K^{-1}]
$\boldsymbol{dl}$	=	Infinitesimal length	[m]
$\boldsymbol{E}$	=	electric field intensity	[V.m^{-1}]
$\boldsymbol{f_e}$	=	electromagnetic force	[N.m^{-3}]
$\boldsymbol{g}$	=	acceleration due to gravity	[m.s^{-2}]
$\boldsymbol{H}$	=	magnetic field	[A.m^{-1}]
$\boldsymbol{I}$	=	total current flowing through metal bath	[A]
$\boldsymbol{j}$	=	electric current density	[A.m^{-2}]
k	=	thermal conductivity	[W.m^{-1}.K^{-1}]
L	=	radial distance	[m]
L_0	=	characteristic length (average grid dimension)	[m]
p	=	pressure	[N.m^{-2}]
q	=	surface heat flux below the top electrode	[W.m^{-2}]
Re_m	=	magnetic Reynolds number	[-]
r	=	radial coordinate	[m]
T	=	temperature	[°C]
T_0	=	reference temperature	[°C]
t	=	time	[s]
u, w	=	velocity component in r and z direction	[m.s^{-1}]
U_0	=	characteristic velocity (average velocity)	[m.s^{-1}]
v	=	velocity vector	[m.s^{-1}]
z	=	axial coordinate	[m]
$\Delta x, \Delta z$	=	mesh size along r and z directions	[m]
σ	=	conductivity	[℧.m^{-1}]
ρ	=	density	[kg.m^{-3}]
β	=	co-efficient of thermal expansion	[K^{-1}]
ϕ	=	electric potential	[V]
μ	=	viscosity	[Pa.s]
μ_0	=	electrical permeability	[H/m]

Literature Cited

Bejan, A.; Convection Heat Transfer, John Wiley & Sons, New York (1984)

Hidaka, H., M. Takahashi, H. Ichikawa, J. Sakane, and S. Kobayashi; "Computation Analysis of Flow of Molten Steel in DC Arc Furnace (inJapanese)," *Shinnittetsu Giho*, **No. 342**, 33-37 (1991)

Morisue, T., H. N. Mondal and H. Kurimoto; "Electrically induced flows in DC electric arc furnace," *Proceedings of the autumn meeting of chemical engineers of Japan*, A 306, September (1994)

Nakamura T., N. Ao, and K. Ishihara; "Equipment and Operation Results of 30t DC Arc Furnace at Topy Toyohashi Works (in Japanese)," *Tetsu-to-Hagane*, **77** (4), 520-527 (1991)

Patankar, S. V.; Numerical Heat Transfer and Fluid flow, Hemisphere, New York (1980)

Szekely, J., J. McKelliget, and M. Choudhary; "Heat-transfer fluid flow and bath circulation in electric-arc furnaces and DC plasma furnaces," *Ironmaking and Steelmaking*, **10** (4), 169 (1983)

Ushiro, M., J., Szekely, and C.W. Chang; "Mathematical modelling of flow field and heat transfer in high-current arc discharge," *Ironmaking and steelmaking*, **8** (6), 279 (1981)

Yamada,T., K. Ishida, T. Nakajima, and Y. Namiiri ; "IHI-ABB Type Direct Current Electric Arc Furnace (in Japanese)," *Ishikawajima-Harima Engineering Review*, **31** (4), 274-279 (1991)